Computer Assisted Mechanics and Engineering Sciences, 14: 251–275, 2007.

Neural network aided stochastic computations and earthquake engineering

Nikos D. Lagaros, Manolis Papadrakakis, Michalis Fragiadakis, George Stefanou
Institute of Structural Analysis and Seismic Research, School of Civil Engineering National Technical University Zografou Campus, Athens 15780, Greece

Yiannis Tsompanakis
Division of Mechanics, Department of Applied Sciences, Technical University of Crete University Campus, Chania 73100, Greece

(Received in the final form March 20, 2007)

This article presents recent developments in the field of stochastic finite element analysis of structures and earthquake engineering aided by neural computations. The incorporation of Neural Networks (NN) in this type of problems is crucial since it leads to substantial reduction of the excessive computational cost. In particular, a hybrid method is presented for the simulation of homogeneous non-Gaussian stochastic fields with prescribed target marginal distribution and spectral density function. The presented method constitutes an efficient blending of the Deodatis–Micaletti method with a NN based function approximation. Earthquake-resistant design of structures using Probabilistic Safety Analysis (PSA) is an emerging field in structural engineering. It is investigated the efficiency of soft computing methods when incorporated into the solution of computationally intensive earthquake engineering problems.

1. Introduction

Over the last ten years artificial intelligence techniques like Neural Networks (NN) have emerged as a powerful tool that could be used to replace time consuming procedures in many scientific or engineering applications. The fields where NN have been successfully applied are: (i) pattern recognition, (ii) regression (function approximation/fitting) and (iii) optimization. In the past the first field of application of NN was mostly used for predicting the behavior of a structural system in the context of structural optimal design [13, 15], structural damage assessment [29], the evaluation of buckling loads of cylindrical shells with geometrical imperfections [30] or structural reliability analysis [7, 14, 16]. This study presents recent developments in the applications of NN in the field of stochastic finite element analysis and probabilistic analysis of structures.

Many sources of uncertainty (material, geometry, loads, etc) are inherent in structural design. Probabilistic analysis of structures leads to safety measures that a design engineer has to take into account due to the aforementioned uncertainties. Probabilistic analysis problems, especially when seismic loading is considered, are highly computationally intensive tasks since in order to obtain the structural behaviour a large number of dynamic analyses (e.g modal response spectrum analysis, or nonlinear time-history analysis) are required. In this work two metamodel based applications are considered in order to reduce the aforementioned computational cost. The efficiency of a trained NN is demonstrated, where a network is used to predict maximum interstorey drift values due to different sets of random variables. As soon as the maximum interstorey drift is known, the limit-state probabilities are calculated by means of Monte Carlo Simulation (MCS). In the first application the probability of exceedance of a limit-state is obtained when the Multi-modal Response Spectrum

analysis is adopted [26]. In the second application fragility analysis of a ten-storey moment resisting steel frame is evaluated where limit-state fragilities are determined by means of nonlinear time-history analysis [6].

The problem of simulating non-Gaussian stochastic processes and fields has gained considerable interest in stochastic computational mechanics over the past years. This can be attributed to the fact that several quantities arising in practical engineering problems (e.g. material and geometric structural properties, soil properties in geotechnical engineering applications, etc) exhibit non-Gaussian probabilistic characteristics. Especially the simulation of highly skewed and narrow-banded fields is well recognized nowadays as a benchmark that reveals the limitations of the existing simulation methods [1, 4, 12].

The theory and methods of structural reliability have been developed significantly during the last twenty years and have been documented in an increasing number of publications [24]. In this work the probabilistic safety analysis of framed structures under seismic loading conditions is investigated based on the methodology proposed by Fragiadakis *et al.* [6]. Both randomness of ground motion excitation (that influence the seismic demand level) and material properties (that affect the structural capacity) are taken into consideration. Additionally, a computationally efficient procedure, proposed in a previous work by Lagaros *et al.* [11], for the simulation of homogeneous non-Gaussian stochastic fields with prescribed target marginal distribution and spectral density function is presented. This procedure is based on the method developed by Deodatis and Micaletti [1], which constitutes an improved version of the algorithm proposed by Yamazaki and Shinozuka [28]. Both approaches are related to the translation process concept [4] and are based on the spectral representation method, in the sense that in order to produce sample functions of the underlying Gaussian field they use the spectral representation method.

The assessment of the bearing capacity of framed structures, in terms of maximum interstorey drift, is determined via non-linear time history analysis. Probabilistic Safety Analysis (PSA) using the Monte-Carlo Simulation (MCS) method and non-linear time history analysis results in a highly computationally intensive problem. In order to reduce the computational cost, NN are employed. For the training of the NN a number of Intensity Measures (IMs) are used in order to accurately predict the maximum interstorey drift values. The IMs adopted in the present study can be classified either as seismic record dependent only, or as both structure and record dependent. Via the presented PSA procedure fragility curves are obtained for different hazard levels. In addition the probability of structure's failure is derived as a limit-state function of seismic intensity.

2. Multi-layer perceptrons

A multi-layer perceptron is a feed-forward neural network, consisting of a number of units (neurons) linked together, training attempts to create a desired relation in an input/output set of learning patterns. A learning algorithm tries to determine the weight parameters, in order to achieve the right response for each input vector applied to the network. The numerical minimization algorithms used for the training generate a sequence of weight matrices through an iterative procedure. To apply an algorithmic operator $\mathcal{A}$ a starting weight matrix $w^{(0)}$ is needed, while the iteration formula can be written as follows,

$$w^{(t+1)} = \mathcal{A}(w^{(t)}) = w^{(t)} + \Delta w^{(t)}. \tag{1}$$

All numerical methods applied for the NN training are based on the above formula. The changing part of the algorithm $\Delta w^{(t)}$ is further decomposed into two parts as

$$\Delta w^{(t)} = a_t d^{(t)} \tag{2}$$

where $d^{(t)}$ is a desired search direction of the move and a_t the step size in that direction.

The training methods can be divided into two categories. Algorithms that use global knowledge of the state of the entire network, such as the direction of the overall weight update vector, which

are referred as *global* techniques. In contrast local adaptation strategies are based on weight specific information only such as the temporal behaviour of the partial derivative of this weight. The local approach is more closely related to the NN concept of distributed processing in which computations can be made independent to each other. Furthermore, it appears that for many applications local strategies achieve faster and more reliable predictions than global techniques despite the fact that they use less information [23].

2.1. Global adaptive techniques

The algorithms most frequently used in the NN training are the steepest descent, the conjugate gradient and the Newton's method with the following direction vectors:

- *Steepest descent method*: $d^{(t)} = -\nabla\mathcal{E}(w^{(t)})$,
- *Conjugate gradient method*: $d^{(t)} = -\nabla\mathcal{E}(w^{(t)}) + \beta_{t-1}d^{(t-1)}$ where β_{t-1} is defined as

$$\beta_{t-1} = \nabla\mathcal{E}_t \cdot \nabla\mathcal{E}_t \,/ \nabla\mathcal{E}_{t-1} \cdot \nabla\mathcal{E}_{t-1} \qquad \text{Fletcher–Reeves},$$

- *Newton's method*: $d^{(t)} = -\left[H(w^{(t)})\right]^{-1} \nabla\mathcal{E}(w^{(t)})$.

The convergence properties of the optimization algorithms for differentiable functions depend on the properties of the first and/or second derivatives of the function to be optimized. When optimization algorithms converge slowly for NN problems, this suggests that the corresponding derivative matrices are numerically ill-conditioned. It has been shown that these algorithms converge slowly when rank-deficiencies appear in the Jacobian matrix of a NN, making the problem numerically ill-conditioned [10].

2.2. Local adaptive techniques

To improve the performance of weight updating, two approaches have been proposed, namely Quickprop [2] and Rprop [21].

The Quickprop method

This method is based on a heuristic learning algorithm for a multi-layer perceptron, developed by Fahlman [2], which is partially based on the Newton's method. Quickprop is one of most frequently used adaptive learning paradigms. The weight updates are based on estimates of the position of the minimum for each weight, obtained by solving the following equation for the two following partial derivatives,

$$\frac{\partial\mathcal{E}_{t-1}}{\partial w_{ij}} \qquad \text{and} \qquad \frac{\partial\mathcal{E}_t}{\partial w_{ij}}\,, \tag{3}$$

and the weight update is implemented as follows,

$$\Delta w_{ij}^{(t)} = \frac{\frac{\partial\mathcal{E}_t}{\partial w_{ij}}}{\frac{\partial\mathcal{E}_{t-1}}{\partial w_{ij}} - \frac{\partial\mathcal{E}_t}{\partial w_{ij}}}\,\Delta w_{ij}^{(t-1)}. \tag{4}$$

The learning time can be remarkably improved compared to the global adaptive techniques.

2.2.1. The Rprop method

Another heuristic learning algorithm with locally adaptive learning rates based on an adaptive version of the Manhattan learning rule and developed by Riedmiller and Braun [21] is the **R**esilient back**prop**agation algorithm abbreviated as Rprop. The weight updates can be written as

$$\Delta w_{ij}^{(t)} = -\eta_{ij}^{(t)} \operatorname{sgn}\left(\frac{\partial \mathcal{E}_t}{\partial w_{ij}}\right) \tag{5}$$

where

$$\eta_{ij}^{(t)} = \begin{cases} \min(\alpha \cdot \eta_{ij}^{(t-1)}, \eta_{\max}), & \text{if } \dfrac{\partial \mathcal{E}_t}{\partial w_{ij}} \cdot \dfrac{\partial \mathcal{E}_{t-1}}{\partial w_{ij}} > 0, \\ \max(b \cdot \eta_{ij}^{(t-1)}, \eta_{\min}), & \text{if } \dfrac{\partial \mathcal{E}_t}{\partial w_{ij}} \cdot \dfrac{\partial \mathcal{E}_{t-1}}{\partial w_{ij}} < 0, \\ \eta_{ij}^{(t-1)}, & \text{otherwise,} \end{cases} \tag{6}$$

where $\alpha = 1.2$, $b = 0.5$, $\eta_{\max} = 50$ and $\eta_{\min} = 0.1$ [22]. The learning rates are bounded by upper and lower limits in order to avoid oscillations and arithmetic underflow. It is interesting to note that, in contrast to other algorithms, Rprop employs information about the sign and not the magnitude of the gradient components.

3. Theoretical background for non-Gaussian fields

The methods developed in the literature for the simulation of non-Gaussian stochastic fields can be grouped into two main categories. The methods which belong to the first category, seek to produce sample functions matching the prescribed power spectral density function and lower-order statistics (mean, variance, skewness and kurtosis) of a target stochastic field [5]. However, sample functions having only the prescribed lower moments are not sufficient for the successful solution of problems where the accurate characterization of the tails of the distributions is of importance (e.g. soil liquefaction [19]). This is due to the potential non-uniqueness of the marginal probability distribution of realizations of a non-Gaussian field that is defined only by its lower-order moments. The methods belonging to the second category are more challenging in the sense that they seek to generate sample functions compatible to complete probabilistic information, namely the marginal probability distribution and the spectral density function of the stochastic field [1, 4, 18, 28].

In this work a computationally efficient soft computing hybrid methodology is presented, for the simulation of homogeneous non-Gaussian stochastic fields with prescribed target marginal distribution and spectral density function [11]. The present methodology retains the accuracy characteristics of the method proposed in [1] while drastically reduces the computational effort of the simulation by reliably predicting the unknown underlying Gaussian spectrum.

Since all the joint multi-dimensional density functions are needed to fully characterize a non-Gaussian stochastic field, much of the existing research has focused on a more realistic way of defining a non-Gaussian sample function as a simple transformation of some underlying Gaussian field with known second-order statistics. If $g(x)$ is a homogeneous zero-mean Gaussian field with unit variance and power Spectral Density Function (SDF) $S_{gg}(\kappa)$ (or equivalently autocorrelation function $R_{gg}(\xi)$), a homogeneous non-Gaussian stochastic field $f(x)$ with power spectrum $S_{ff}^{T}(\kappa)$ can be defined as

$$f(x) = F^{-1} \cdot \Phi[g(x)] \tag{7}$$

where Φ is the standard Gaussian cumulative distribution function and F is the non-Gaussian marginal cumulative distribution function of $f(x)$. The transform $F^{-1} \cdot \Phi$ is a memory-less translation

since the value of $f(x)$ at an arbitrary point x depends only on the value of $g(x)$ at the same point and the resulting non-Gaussian field is called a translation field [3, 4]. It is worth noting that Eq. (7) is a Gaussian to non-Gaussian mapping and that $f(x)$ has also zero-mean and unit variance.

The main difficulty when dealing with translation fields is that, although the mapped sample functions of Eq. (7) will have the prescribed target marginal probability distribution F, their SDF will not be identical to $S_{ff}^{T}(\kappa)$ due to the non-linearity of the mapping. Another important issue pointed out by Grigoriu [4] is that the choice of the marginal distribution of $f(x)$ imposes constrains to its correlation structure reflected by the relationship

$$R_{ff}(\xi) = \int_{-\infty}^{\infty}\int_{-\infty}^{\infty} F^{-1}[\Phi(g_1)]\, F^{-1}[\Phi(g_2)] \cdot \phi[g_1, g_2; R_{gg}(\xi)]\, \mathrm{d}g_1 \mathrm{d}g_2 \tag{8}$$

where $g_1 = g(x)$, $g_2 = g(x+\xi)$ and $\phi[g_1, g_2; R_{gg}(\xi)]$ denotes the joint density of $\{g_1, g_2\}$.

Strictly speaking, if the target F and $R_{ff}^{T}(\xi)$ are proven to be incompatible from Eq. (8), there is no translation field with the prescribed characteristics. The relationship between the two autocorrelation functions (or equivalently between the two power spectra) can have a closed form only in few cases (e.g. lognormal and cubic fields) [4]. The problem of incompatibility becomes even greater for highly skewed narrow-banded stochastic fields as it is explained in [1]. In this case, one has to resort to translation fields that match the target marginal distribution and SDF approximately. The particular approximation mainly depends on the nature of the problem considered. An accurate recreation of the tails of the probability density function (PDF) may be critical in fatigue analysis or in soil liquefaction problems whereas capturing a narrow-banded SDF may be crucial in the analysis of a lightly damped system [12, 19].

4. Simulation algorithms

The two aforementioned problems arising in the context of translation fields have been studied in the last decade by several researchers [1, 4, 12]. The solutions proposed by Yamazaki–Shinozuka [28] and Deodatis–Micaletti [1] are briefly discussed in the following lines together with the respective algorithms.

4.1. Yamazaki–Shinozuka (Y-S) algorithm

In order to address the problem of spectral distortion caused by the nonlinear transformation of Eq. (7), Yamazaki and Shinozuka proposed an iterative procedure involving the repeated updating of the SDF of the underlying Gaussian stochastic field $g(x)$. This updating process is defined in such a way that when the final realization of $g(x)$ is generated according to the updated $S_{gg}(\kappa)$ and then mapped to $f(x)$ via Eq. (7), the resulting non-Gaussian sample function will have both the prescribed marginal probability distribution and SDF. The formula used to update $S_{gg}(\kappa)$ is the following,

$$S_{gg}^{(j+1)}(\kappa) = \frac{S_{gg}^{(j)}(\kappa)}{S_{ff}^{(j)}(\kappa)}\, S_{ff}^{T}(\kappa), \tag{9}$$

where j is an iteration index. The rationale existing behind the choice of this expression is that the rate of change at each wave number, which is represented by the ratio $S_{gg}^{(j)}(\kappa)/S_{ff}^{(j)}(\kappa)$, is expected to approach a constant value after a small number of iterations. The issue of possible incompatibility between the target F and $R_{ff}^{T}(\xi)$ (or $S_{ff}^{T}(\kappa)$) has not been addressed and the two quantities are arbitrarily defined in the algorithm.

The Y-S algorithm can be summarized as follows:

- Generation of a Gaussian sample function using the spectral representation method,

$$g(x) = 2 \sum_{n=0}^{N-1} \sqrt{S_{gg}(\kappa_n)\, \Delta\kappa}\, \cos(\kappa_n x + \phi_n) \tag{10}$$

(for the first iteration, the relationship $S_{gg}(\kappa) = S_{ff}^{T}(\kappa)$ is used).

- Calculation of the corresponding non-Gaussian sample function using Eq. (7).

- Estimation of the SDF of the non-Gaussian sample function via spatial averaging,

$$S_{ff}^{(j)}(\kappa) = \left| \frac{1}{2\pi T} \int_0^T f^{(j)}(x) \exp(-i\kappa x)\, \mathrm{d}x \right|^2 . \tag{11}$$

- Convergence checking: $S_{ff}^{(j)}(\kappa) \stackrel{?}{=} S_{ff}^{T}(\kappa)$. If not, updating of $S_{gg}(\kappa)$ is performed via Eq. (9).

This algorithm provides fairly good results for slightly non-Gaussian fields with broad-banded SDFs. For the case of highly skewed and/or narrow-banded fields, several issues arise regarding the Gaussianity and homogeneity of the Gaussian sample functions produced by Eq. (10). These issues are discussed in the following section.

4.2. Deodatis–Micaletti (D-M) algorithm

Deodatis and Micaletti [1] pointed out that the previous algorithm presents some limitations especially with regard to the simulation of highly skewed non-Gaussian stochastic fields. These limitations are due to the specific form of the updating formula of Eq. (9). The major problem is that after the first iteration the underlying Gaussian field is no more Gaussian and homogeneous. This departure from Gaussianity and homogeneity can be briefly explained as follows: Since $S_{gg}^{(j+1)}(\kappa)$ is related with $S_{ff}^{(j)}(\kappa)$ and since $S_{ff}^{(j)}(\kappa)$ depends on the random phase angles ϕ_n due to Eq. (11), the terms in series of Eq. (10) are not independent. The central limit theorem clearly states that the terms in the summation have to be independent in order for $g(x)$ to be asymptotically Gaussian as $N \to \infty$. The authors observed that, for highly skewed marginal probability distributions, the correlations between the terms of Eq. (10) can become strong leading to a substantially non-Gaussian and non-homogeneous underlying field (although the deviation from homogeneity was found to be much smaller than the deviation from Gaussianity). As a result of these deviations, the generated non-Gaussian sample functions will not have the prescribed marginal PDF.

Having in mind the aforementioned observations, Deodatis and Micaletti proposed an algorithm having the same structure as the previous one but with the following improvements:

- The updating scheme has been slightly modified in order to achieve more rapid convergence,

$$S_{gg}^{(j+1)}(\kappa) = \left[\frac{S_{ff}^{T}(\kappa)}{S_{ff}^{(j)}(\kappa)} \right]^{\alpha} S_{gg}^{(j)}(\kappa). \tag{12}$$

From extensive experimentation, the authors concluded that a value of α equal to 0.3 gives the better results in terms of convergence.

- In order to overcome the problems resulting from the specific form of the updating scheme, Eq. (7) has been extended to an empirical non-Gaussian to non-Gaussian mapping quantifying at every iteration the deviation from Gaussianity of the underlying "Gaussian" field

$$f(x) = F^{-1} \cdot F^*[g(x)] \tag{13}$$

where F^* is the empirical marginal probability distribution of $g(x)$ updated in each step.

- The issue of possible incompatibility between the target F and $R_{ff}^T(\xi)$ has been addressed by using a "spectral preconditioning" step based on Eq. (8) and leading in some cases to slight modifications of the spectral content of the prescribed SDF. The resulting modified spectrum is used for starting the procedure.

- The sample functions produced by Eq. (10) are frequency shifted i.e. the values of the SDF at wave numbers $\kappa_n = n\Delta\kappa + \Delta\kappa/2$ are employed instead of the values at $\kappa_n = n\Delta\kappa$ [31]. This modification is introduced only for simulation purposes in order to circumvent some convergence issues arising around $\kappa = 0$.

The D-M algorithm provides sample functions that match the prescribed characteristics with remarkable accuracy even in the case of non-Gaussian fields with large skewness and narrow-banded spectra. However, the use of the updating formula of Eq. (12) in conjunction with the iterative calculation of the empirical distribution of the underlying "Gaussian" field significantly burdens the computational cost of the algorithm.

5. Fragility analysis using Monte Carlo simulation

Extreme earthquake events may produce extensive damage to structural systems despite their low probabilities of occurrence. It is therefore essential to establish a reliable procedure for assessing the seismic risk of real-world structural systems. Probabilistic safety analysis provides a rational framework for taking into account the various sources of uncertainty that may influence structural performance under seismic loading conditions. The core of PSA is seismic fragility analysis, which provides a measure of the safety margin of a structural system for different limit-states.

The theory and the methods of structural reliability have been developed significantly during the last twenty years and are documented in a large number of publications [24]. In this work the probabilistic safety analysis of framed structures under seismic loading conditions is investigated. Randomness of ground motion excitation (that influences seismic demand) and of material properties (that affect structural capacity) are taken into consideration using Monte Carlo Simulation. The capacity assessment of steel frames is determined using nonlinear time-history analysis. The probabilistic safety analysis using Monte-Carlo Simulation and nonlinear time history analysis results in a computationally intensive problem. In order to reduce the excessive computational cost, techniques based on NN are implemented. For the training of the NN a number of IMs are derived from each earthquake record, for the prediction of the level of damage, which is measured by means of maximum interstorey drift values $\theta_{\max}$.

The seismic fragility of a structure $F_R(x)$ is defined as its limit-state probability, conditioned on a specific peak ground acceleration, spectral velocity, or other control variable that is consistent with the specification of seismic hazard

$$F_R(x) = P[LS_i/PGA = x] \tag{14}$$

where LS_i represents the corresponding i-th limit-state and the peak ground PGA is the control variable. If the annual probabilities of exceedance $P[PGA = x]$ of specific levels of earthquake motion

are known, then the mean annual frequency of exceedance of the i-th limit-state is calculated as follows,

$$\lambda_{LS_i} = \sum_x F_R(x)\, P[PGA{=}x]. \tag{15}$$

Equation (15) can be used for taking decisions about, for example, the adequacy of a design or the need to retrofit a structure. In the present study the aim is to evaluate the fragility $F_R(x)$. Once the fragility is calculated the extension to Eq. (15) is straightforward.

Often $F_R(x)$ is modelled with a lognormal probability distribution, which leads to an analytic calculation. In the present study Monte Carlo Simulation (MCS) with improved Latin Hypercube Sampling (iLHS) for the reduction of the sampling size, is adopted for the numerical calculation of $F_R(x)$. Numerical calculation of Eq. (14) provides a more reliable estimate of the limit-state probability, since it is not necessary to assume that seismic data follow a lognormal distribution. However, in order to calculate the limit-state probability, a large number of nonlinear dynamic analyses are required for each hazard level, especially when the evaluation of extremely small probabilities is needed.

The methodology requires that MCS has to be performed at each hazard level. Earthquake records are selected randomly and scaled to a common intensity level that corresponds to the hazard level examined. Scaling is performed using the first mode spectral acceleration of the 5% damped spectrum ($Sa(T_1, 5\%)$). Therefore, all records are scaled in order to represent the same ground motion intensity in terms of $Sa(T_1, 5\%)$. Earthquake loading is considered as two separate sources of uncertainty, ground motion intensity and the details of ground motion. The first uncertainty refers to the general severity of shaking at a site, which may be measured in terms of any IM such as PGA, $Sa(T_1, 5\%)$, Arias intensity, etc. The second source refers to the fact that, although different acceleration time histories can have their amplitudes scaled to a common intensity, there is still uncertainty in the performance, since IMs are imperfect indicators of the structural response. The first source is considered by scaling all records to the same intensity level at each limit-state. The second source is treated by selecting natural records as random variables from a relatively large suite of scenario based records. The concept of considering separately seismic intensity and the details of ground is the backbone of the Incremental Dynamic Analysis (IDA) method [27], while Porter *et al.* [20] have also introduced intensity and different records as two separate uncertain parameters in order to evaluate the sensitivity of structural response to different uncertainties.

The random parameters considered in this study are the material properties and more specifically the modulus of elasticity E and the yield stress f_y, as well as and the details of ground motion where a suite of scenario based earthquake records is used. The material properties are assumed to follow the normal distribution while the uniform distribution is assumed for the records in order to select them randomly from a relatively large bin of natural records. The first two variables are sampled by means of the iLHS technique in order to increase the efficiency of the sampling process.

In reliability analysis the MCS method is often employed when the analytical solution is not attainable and the failure domain can not be expressed or approximated by an analytical form. This is mainly the case in problems of complex nature with a large number of basic variables where all other reliability analysis methods are not applicable. Expressing the limit-state function as $\mathbf{G}(\mathbf{x}) < 0$, where $\mathbf{x} = (x_1\,, x_2\,, \ldots, x_M)^T$ is the vector of the random variables, the probability of exceedance can be obtained as

$$P_{LS} = \int_{G(x)\geq 0} f_x(x)\, \mathrm{d}x \tag{16}$$

where $f_x(\mathbf{x})$ denotes the joint probability of failure for all random variables. Since MCS is based on the theory of large numbers (N_∞) an unbiased estimator of the probability of failure is given by

$$P_{LS} = \frac{1}{N_\infty} \sum_{j=1}^{N_\infty} I(x_j) \tag{17}$$

where $I(\mathbf{x}_j)$ is a Boolean vector indicating failure and non-failure simulations. In order to estimate P_{LS} an adequate number of N_{sim} independent random samples is produced using a specific probability density function for the vector $\mathbf{x}$. The value of the failure function is computed for each random sample x_j and the Monte Carlo estimation of P_{LS} is given in terms of the sample mean by

$$P_{LS} \cong \frac{N_H}{N_{\text{sim}}} \tag{18}$$

where N_H is the number of failure simulations, where the maximum interstorey drift value exceeds a threshold drift for the limit-state examined. In order to calculate Eq. (18) N_{sim} nonlinear time history analyses have to be performed at each hazard level. Clearly the computational cost of performing so many nonlinear dynamic analyses, even when an efficient sampling reduction technique (such as iLHS) is used, is prohibitive. In order to reduce the computational cost, properly trained NN are implemented.

As already mentioned back-propagation NN are used in order to reduce the number or earthquake simulations required for the calculation of the probability of Eq. (18). The principal advantage of a properly trained NN is that it requires a trivial computational effort to produce an acceptable approximate solution. Such approximations appear to be valuable in situations where actual response computations are CPU intensive and quick estimations are required. Neural networks have been applied in the past by Papadrakakis *et al.* [16] in order to calculate the probability of failure for steel moment frames using inelastic static analysis. In recent studies NN have been adopted for the reliability analysis of structures by Nie and Ellingwood [14] and Hurtado [8]. However, in the present study the NN are implemented in order to predict the maximum seismic response with natural earthquake records replacing the time consuming nonlinear time history analysis. The NN are trained in order to predict the maximum interstorey drift $\theta_{\max}$ for different earthquake records which are identified by NN using a set of IMs.

The term Intensity Measure is used to denote a number of common ground motion parameters which represent the amplitude, the frequency content, the duration or any other ground motion parameter. A number of different IMs has been presented in the literature [9], while various attempts to relate an IM with a damage measure such as maximum interstorey drift values have been made [25]. The IMs adopted can be classified as record dependent only or as both structure and record dependent. The complete list of the IMs used in this study is given in Table 1.

It can be seen that the IMs selected, vary from widely used ground motion parameters such as peak ground acceleration (PGA) to more sophisticated measures such as SaC. The definitions and

Table 1. Intensity measures

No	Intensity Measure
1	PGA (g)
2	PGV (m)
3	PGD (m)
4	V/A (sec)
5	Arias intensity (m/sec)
6	Significant duration (5 to 95 % of Arias) (sec)
7	RMS acceleration (g)
8	Characteristic Intensity
9	CAV
10	Spectral Intensity
11	Total Duration (sec)
12	SA(T_1) (g)
13	SV(T_1) (cm)
14	SaC, $c = 2$ (g)
15	SaC, $c = 3$ (g)

further discussion on the first thirteen measures of Table 1 is given by Kramer [9]. The last two IMs refer to a measure that can be defined as

$$SaC = Sa(T_1)\sqrt{\frac{Sa(c \cdot T_1)}{Sa(T_1)}}. \tag{19}$$

The parameter c takes the value 2 and 3 for the 14th and the 15th parameter of Table 1, respectively. These IMs were introduced in order to assist the NN to capture the effects of inelasticity by considering the elastic spectrum at an "effective" period longer than T_1 , thus reflecting the reduction in stiffness.

For each hazard level separate training of the NN is performed by means of the above IMs. The training process is based on the fact that the trained NN will assign small weights to the IMs which have poor correlation with the damage measure selected. Instead of using the whole set it was examined the suitability of using only some of the IMs of Table 1. The parametric study was performed for various intensity levels since the performance of an IM depends also on the level of nonlinearity that the structure has undergone. The ten combinations of IMs, shown in Table 2, were compared.

Table 2. Intensity measures combinations

ID	IM combinations
A	1
B	1,2
C	1,2,3
D	1,2,3,5
E	1,2,3,5,9
F	1,2,3,5,9,10
G	1,2,3,5,9,10,12
H	1,2,3,5,9,10,12,14
I	1,2,3,5,9,10,12,14,15
J	ALL

Table 3. Prediction errors for the maximum interstorey drift $\theta_{\max}$

	IM Combination									
	A	**B**	**C**	**D**	**E**	**F**	**G**	**H**	**I**	**ALL**
					PGA = 0.05g					
MAX	49.7	39.6	19.6	32.6	15.9	14.8	4.9	27.0	23.6	9.0
MIN	4.4	0.2	0.9	0.3	0.3	0.6	1.0	1.8	0.6	0.3
AVERAGE	26.2	11.0	7.8	7.6	6.6	6.3	2.9	8.5	7.9	4.4
					PGA = 0.27g					
MAX	32.6	28.2	21.4	26.6	46.7	23.6	9.5	24.5	35.9	9.6
MIN	0.9	0.1	1.1	0.5	1.4	0.1	0.6	0.7	0.3	1.5
AVERAGE	16.9	15.7	11.1	13.3	13.4	9.3	5.0	10.3	9.9	5.0
					PGA = 0.56g					
MAX	62.0	67.2	28.8	42.2	35.4	28.0	33.2	29.3	16.4	9.2
MIN	6.7	3.2	0.2	0.6	0.1	0.2	0.7	1.3	2.2	0.8
AVERAGE	22.8	26.8	10.7	13.1	18.2	14.3	11.1	10.5	7.5	4.8
					PGA = 0.90g					
MAX	72.1	45.2	51.0	23.3	13.3	16.9	12.0	8.7	12.5	9.2
MIN	3.0	6.1	1.4	0.5	1.2	0.9	0.5	0.6	0.2	0.9
AVERAGE	35.9	19.8	18.4	6.8	4.9	8.7	3.8	3.9	4.4	3.8

The performance of each combination is shown in Table 3. The efficiency of the NN is evaluated for the ten-storey steel moment resisting frame described in one of the next sections. For this parametric study the material random variables were considered with their mean values. From Table 3 it is clear that the use of record dependent only measures, such as *PGA*, lead to increased error values, while more refined measures help to reduce the error considerably. The use of the complete set of IMs in Table 1 is preferred since it performed equally well for all four hazard levels examined in the parametric study that follows.

6. Application of the hybrid method for simulating non-Gaussian fields

The aim of this part of the study is to present a soft computing hybrid methodology for simulating in a computationally efficient way homogeneous non-Gaussian stochastic fields with prescribed target marginal distribution and spectral density function. The soft computing hybrid method constitutes an efficient blending of the D-M method with a NN based function approximation. This approach takes advantage of the improvements introduced by Deodatis and Micaletti in [1], while by approximating the unknown Gaussian spectrum with a NN prediction reduces drastically the computational effort of the simulation. This is of paramount importance in the framework of a stochastic structural analysis performed with the Monte Carlo simulation method where, in every simulation, a new non-Gaussian sample function has to be created. The main idea of the presented method is to replace the updating scheme of the Gaussian spectrum of Eq. (12) (source of all important difficulties described in previous sections) by a regression model. Specifically, a Gaussian spectrum is being built using a NN based regression model $\mathcal{H}$. This model has to lead, through Eqs. (10), (11), (13) to a non-Gaussian spectrum consistent to the target spectrum.

It must be noted that, in the hybrid methodology, NN are not implemented according to the classical three-phase procedure: training, testing and prediction phases. The present NN implementation has two distinctive features compared to the conventional one. The first feature is that only the training phase is employed with the training set consisting of one training pair. The input vector corresponds to N wave number values κ while the target vector corresponds to the N values of the target non-Gaussian spectrum. N is the number of points in the discretization of the wave number domain or equivalently the number of terms in the series of cosines formula of Eq. (10). The second feature is that the output and target vectors are different. The output vector corresponds to the unknown Gaussian spectrum while the target vector to the known non-Gaussian spectrum.

The term hybrid stems from the combination of NN with the transformation procedure of Eqs. (10), (11), (13). The training procedure of the hybrid algorithm changes the parameters of the NN (weights) until the prediction of the Gaussian spectrum becomes the "correct" one. In each training step, using Eqs. (10), (11), (13), a non-Gaussian spectrum is produced that matches the target one under the convergence criterion

$$\mathcal{E}(w) = \frac{1}{2}\sum_{j=1}^{N}\left[S_{ff}(\kappa_j) - S_{ff}^{T}(\kappa_j)\right]^2. \tag{20}$$

A schematic representation of the hybrid method is given in Fig. 1.

In this way, the unwanted correlations arising between the terms of the spectral representation series become negligible and thus, the use of translation fields is possible. However, the authors preferred to utilize the extended empirical non-Gaussian to non-Gaussian mapping of Eq. (13) for two main reasons: The first one is related to the inherent limitations associated with the translation field concept, namely the possible incompatibility between the marginal distribution and the correlation structure of a translation field. Since experimental data can lead to a theoretically incompatible pair of F and $R_{ff}^{T}(\xi)$, it is obvious that an algorithm covering a wider range of non-Gaussian fields is preferable. The second reason is connected to the asymptotical Gaussian nature of sample functions produced by the spectral representation method. As the central limit theorem states, an infinite

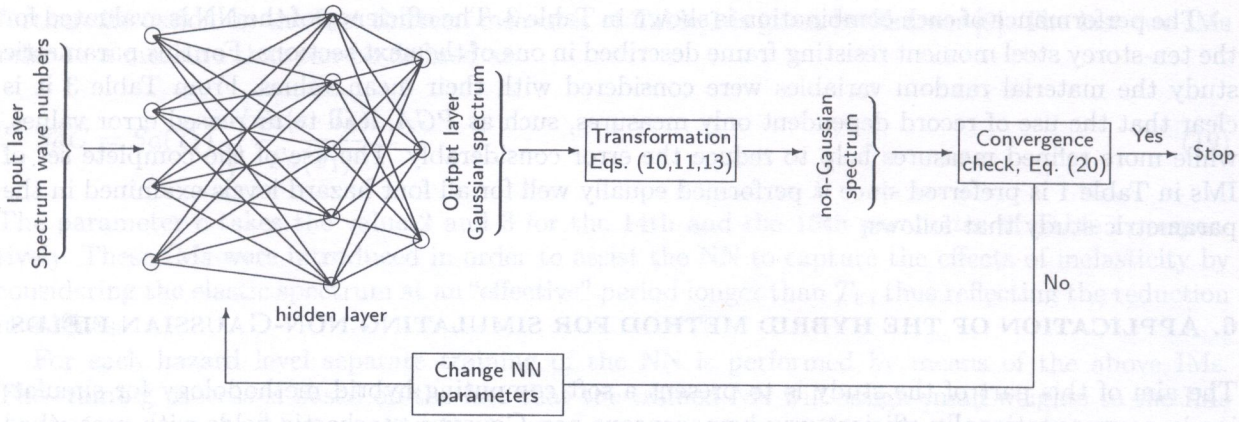

Fig. 1. A schematic representation of the hybrid method

number of terms is required in spectral representation series in order for the generated sample functions to be Gaussian. Since in practical applications a finite number of terms are used, the sample functions are approximately Gaussian and Eq. (10) is always approximate. As a result of the selected mapping (see Eq. (13)), the presented methodology does not require a "spectral preconditioning" step, the relative importance of which, has already been recognized by Deodatis and Micaletti.

At this point, it is worth noting that, especially in the case of highly skewed non-Gaussian fields, omission of the "spectral preconditioning" step leads to a less stable convergence in the D-M method, often requiring a reseeding with another Gaussian sample function to proceed. This means that the overall iterative procedure may be repeated a number of times before reaching convergence. When dealing with stochastic fields with distributions close to the Gaussian, the problem is not so important in contrast to the highly skewed cases, which can require a large number of repeated cycles. The necessity of reseeding in these cases can be explained by the fact that, after a reasonable number of iterations, the updating scheme of Eq. (12) does not lead to any further improvement in $S_{ff}(\kappa)$ and the D-M algorithm continues without converging. The presented methodology, based on the robust updating of the Gaussian spectrum using NN, does not require a reseeding and thus leads to a drastic reduction in the total number of iterations, which over-counterbalance the additional computational cost of the calculation of the empirical marginal probability distribution of $g(x)$ in every iteration.

Furthermore, it has to be pointed out that the presented method takes advantage of the frequency shifting theorem, which further enhances its convergence behavior. In the numerical example presented below, it will be shown that the new approach permits a perfect matching of both target PDF and SDF of highly skewed non-Gaussian fields in a minimum number of iterations, a fact that is very important for the stochastic analysis of real world structures where a large number of sample functions is often needed.

In order to demonstrate the capabilities of the new methodology, a characteristic example is presented involving a highly skewed lognormally distributed field. The stochastic field is homogeneous and has zero mean and unit standard deviation. The correlation structure of the field is described by the following SDF,

$$S_{ff}^{T}(\kappa) = \frac{1}{4}\sigma^2 b^3 \kappa^2 \exp[-b|\kappa|], \qquad \kappa \in R, \tag{21}$$

where σ is the standard deviation of the stochastic field and b denotes a parameter that influences the shape of the spectrum and hence the scale of correlation. It is reminded that, as b increases the SDF becomes more narrow-banded i.e. it has substantial values only in a restricted range of wave numbers. In this example, the values of $\sigma = 1$ and $b = 5$ are selected, leading to a moderately narrow target power spectrum. Finally, the stochastic field has the following characteristics: lognormal marginal probability distribution function defined in the region $[-1.3, 10.0]$, skewness coefficient $= 2.763$ and

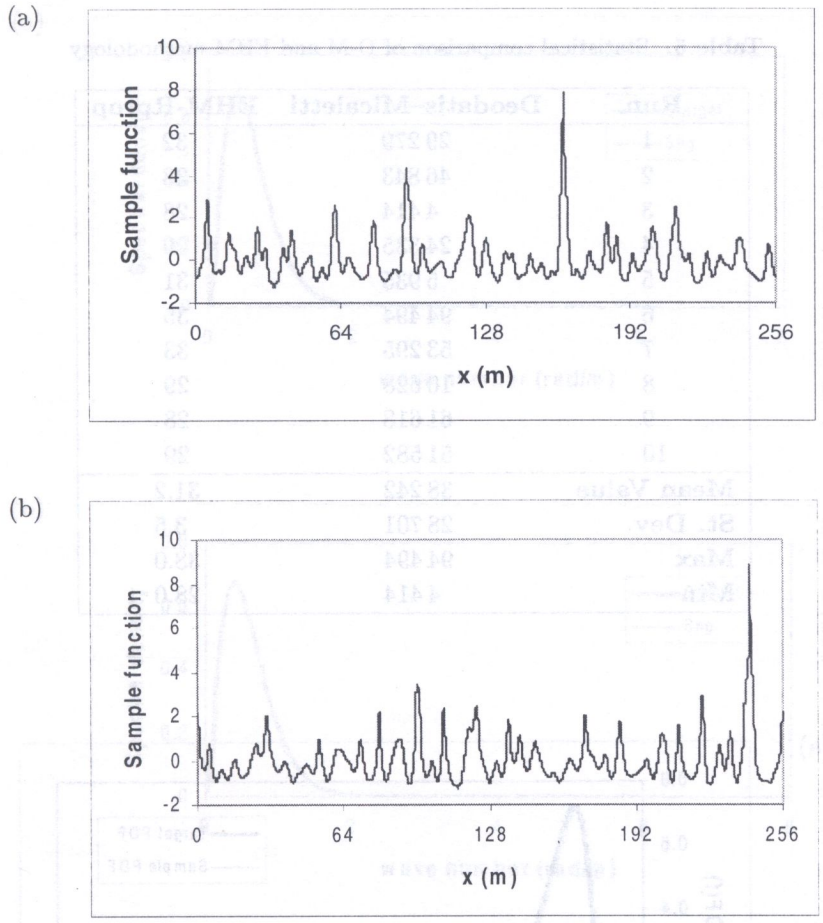

Fig. 2. Sample function generated using (a) Deodatis-Micaletti algorithm, (b) The EHM methodology

Table 4. Computational performance of D-M and EHM methodology

Method	Iterations	Time (sec)
Deodatis–Micaletti	29 279	146
EHM-SD	82	2.0
EHM-CG (Fletcher–Reeves)	25	0.6
EHM-Quickprop	45	1.2
EHM-Rprop	32	0.8

kurtosis coefficient = 19.085. The stochastic field can be characterized as highly skewed since its skewness coefficient is very far from zero.

Sample functions of this numerical test are generated using the D-M and the new methodology (EHM). The FFT version of series of Eq. (10) is used for the generation of the underlying Gaussian field with $N = 128$, $M = 1024$ and upper cut-off wave number $\kappa_u = 6.28\,\mathrm{rad/m}$. A sample function of this numerical test produced by the D-M method is plotted in Fig. 2a while a sample function resulting from the methodology of Lagaros *et al.* [11] is depicted in Fig. 2b. The two sample functions have their values lying within the following ranges:

- Deodatis–Micaletti (Fig. 2a): $[-1.23, 7.87]$,
- EHM methodology (Fig. 2b): $[-1.25, 8.89]$.

These ranges are confirmed by the marginal PDF plots presented below (f-axis). In order to achieve convergence, the D-M algorithm requires a very large total number of iterations while the method of

Table 5. Statistical comparison of D-M and EHM methodology

Run	Deodatis–Micaletti	EHM-Rprop
1	29 279	32
2	46 843	38
3	4 414	28
4	24 335	29
5	5 935	31
6	94 494	35
7	53 295	33
8	10 628	29
9	61 618	28
10	51 582	29
Mean Value	38 242	31.2
St. Dev.	28 701	3.5
Max	94 494	38.0
Min	4 414	28.0

(a)

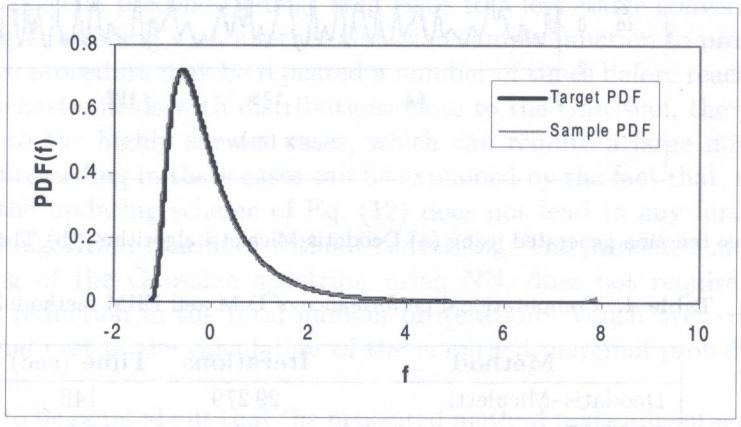

(b)

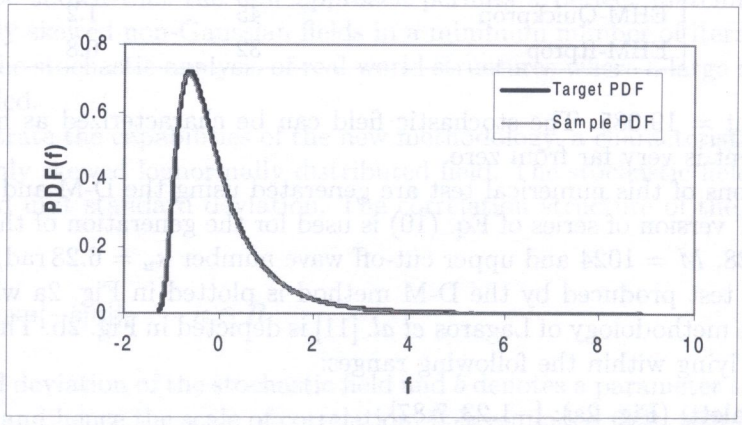

Fig. 3. (a) Marginal PDF of sample function shown in Figure 2a versus target lognormal PDF, (b) Marginal PDF of sample function shown in Figure 2b versus target lognormal PDF

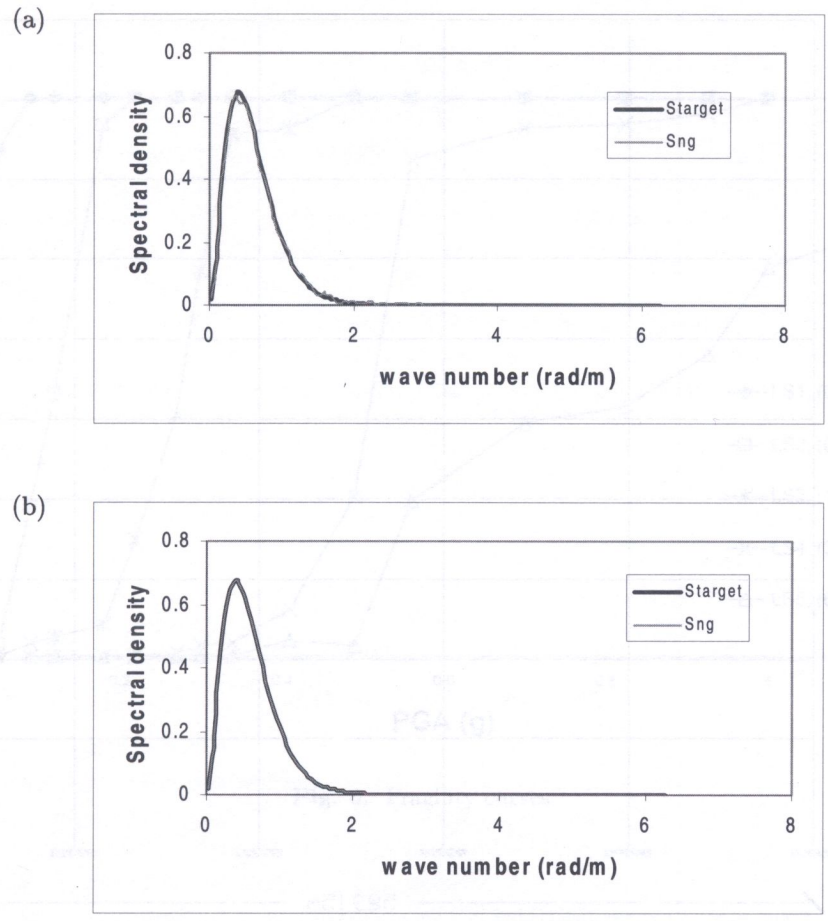

Fig. 4. (a) SDF of sample function shown in Figure 2a versus target SDF, (b) SDF of sample function shown in Figure 2b versus target SDF

Lagaros *et al.* [11] converges in less than 40 iterations. The total computing time of both approaches is given in Table 4. As expected, the time required by the new approach is drastically reduced (about two orders of magnitude less than the time required by the D-M algorithm). The dependence of the two algorithms on the random seed is examined in Table 5 where ten different values of seed are used for starting the procedures.

The marginal PDFs of the two non-Gaussian sample functions are now depicted in Fig. 3. It can be seen that the two approaches provide a very good matching of the target PDF. The SDFs of the two non-Gaussian sample functions are plotted in Fig. 4 along with the corresponding target SDF. The D-M method leads to a good prediction of the target spectrum. For the case of the soft computing based method the Rprop training leads to a perfect matching of the target SDF.

7. Application of NN-based seismic fragility analysis

A suite of 95 scenario-based natural records were used in this study. In order to obtain the fragility curves, sixteen hazard levels expressed in PGA terms ranging from $0.05g$ to $1.25g$ were used. For each hazard level, risk assessment is performed and five limit-state fragilities are calculated. Each limit-state is defined by means of a corresponding maximum interstorey drift $\theta_{\max}$ value. In the present study the five limit-states considered range from serviceability, to life safety and finally to the onset of collapse. The corresponding $\theta_{\max}$ threshold values range from 0.2 to 6 percent.

The test example considered to demonstrate the efficiency of the procedure is the five-bay, ten-storey moment resisting plane frame of Fig. 5. The mean values of the modulus of elasticity is equal

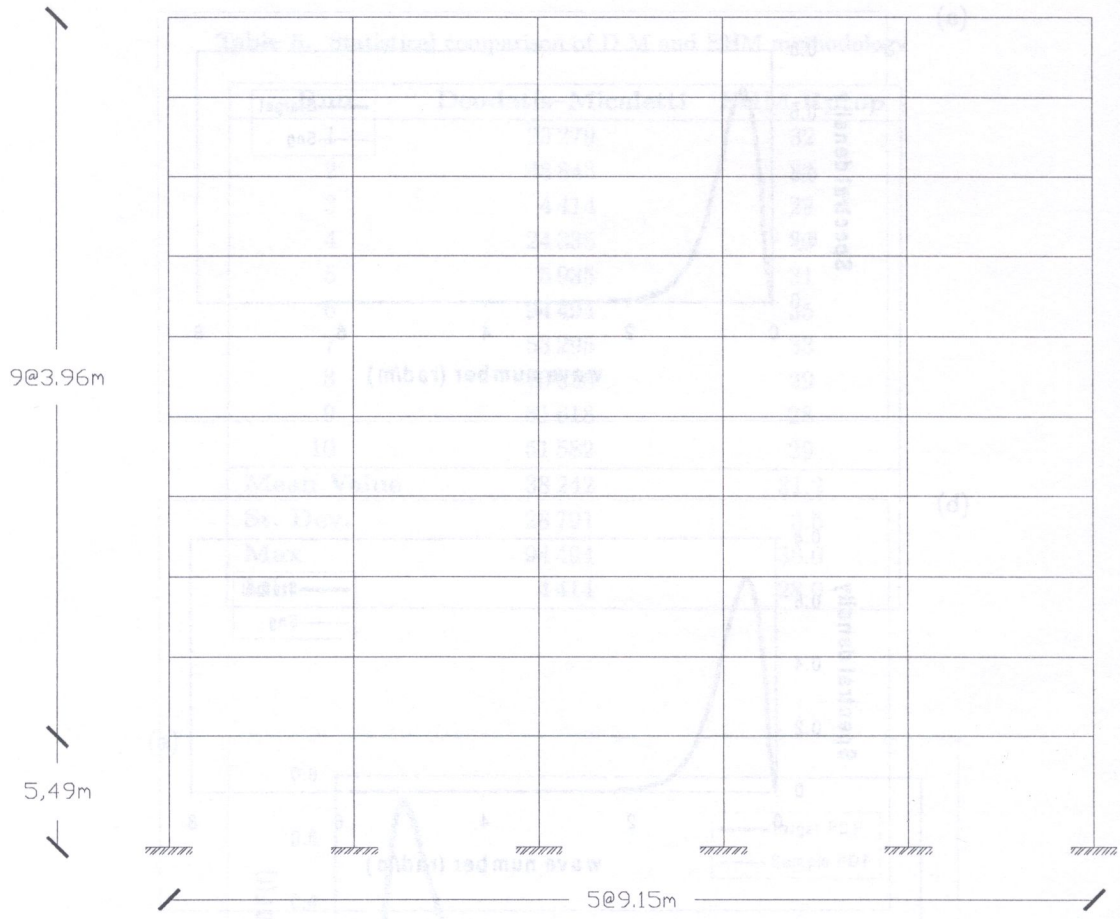

Fig. 5. Ten-storey steel moment frame

to 210 GPa and the yield stress is $f_y = 235\,\text{MPa}$. The coefficients of variation for E and f_y are considered as 5% and 10%, respectively. The constitutive law is bilinear with a strain hardening ratio of 0.01, while the frame is assumed to have rigid connections and fixed supports. The permanent load is equal to $5\,\text{kN/m}^2$ and the live load is taken as $Q = 2\,\text{kN/m}^2$. The gravity loads are contributed from an effective area of 5 m. All analyses were performed using a force-based fiber beam-column element [17] that allows the use of a single element per member, while the same material properties are used for all the members of the frame.

For training the NN both training and testing sets have to be selected for each hazard level. The selection of the sets is based on the requirement that the full range of possible results has to be taken into account in the training step. Therefore, training/testing triads of the material properties and the records are randomly generated using the Latin Hypercube sampling. In the case of earthquake records the selection has to take into account that the scaling factor should be between 0.2 and 5. This restriction is applied because large scaling factors are likely to produce unrealistic earthquake ground motions. Furthermore, the records selected for generating the training set have to cover the whole range of structural damage for the hazard level in consideration. Thus, nonlinear time history analyses were performed, for mean E and f_y values, where the $\theta_{\max}$ values of each record that satisfy the previous requirement were determined for each hazard level. In total 30 records are selected for generating the training set of each hazard level taking into account that the selection has to cover the whole range of $\theta_{\max}$ values. Therefore, training sets with 90 triads of E, f_y and record number, all sampled as discussed above, are generated. Finally, a testing sample of 10 triads is also selected in a similar way in order to test the performance of the NN.

The fragility curves obtained for the five limit-states considered are shown in Fig. 6. Figure 7 shows the number of MCS simulations required for the fragility curve of the Near Collapse limit-

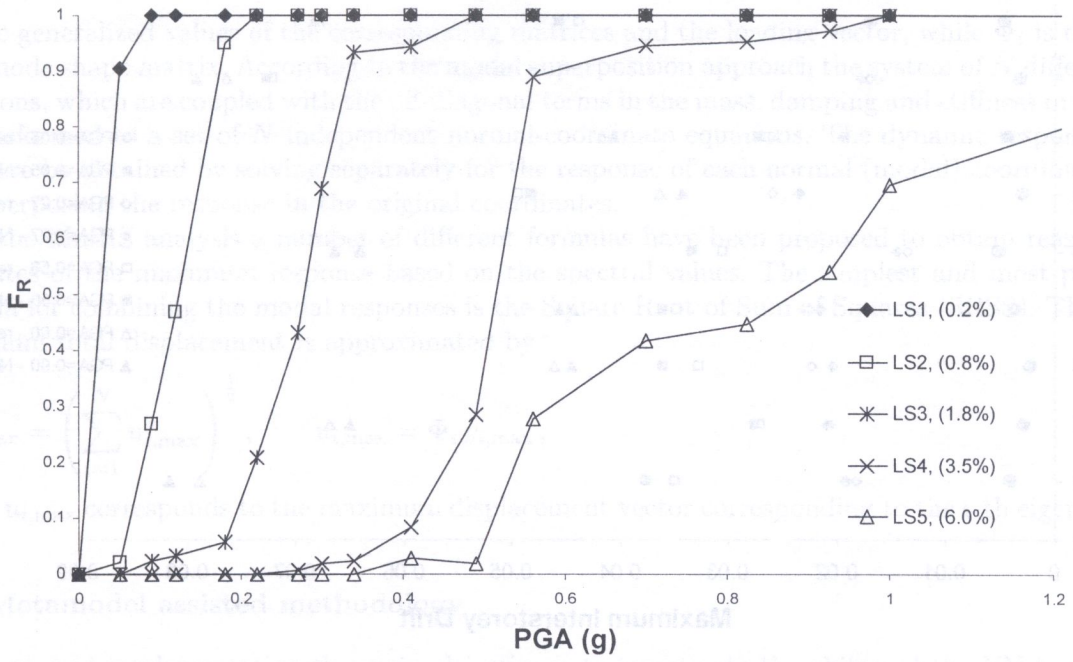

Fig. 6. Fragility curves

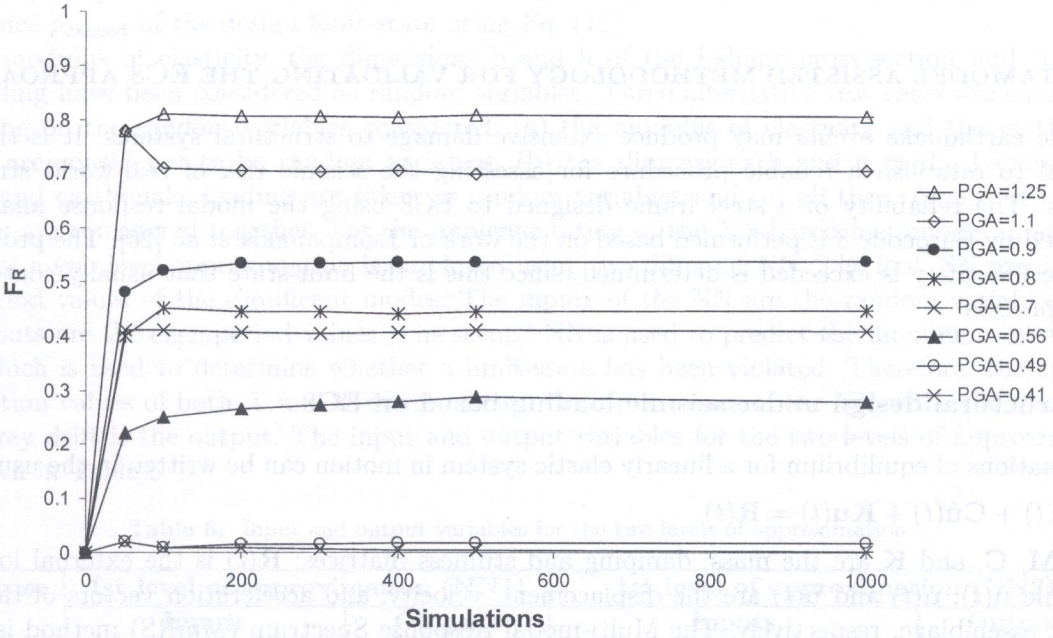

Fig. 7. Number of NN-Simulations required (Near collapse limit-state, $\theta_{\max} \geq 6.0\%$)

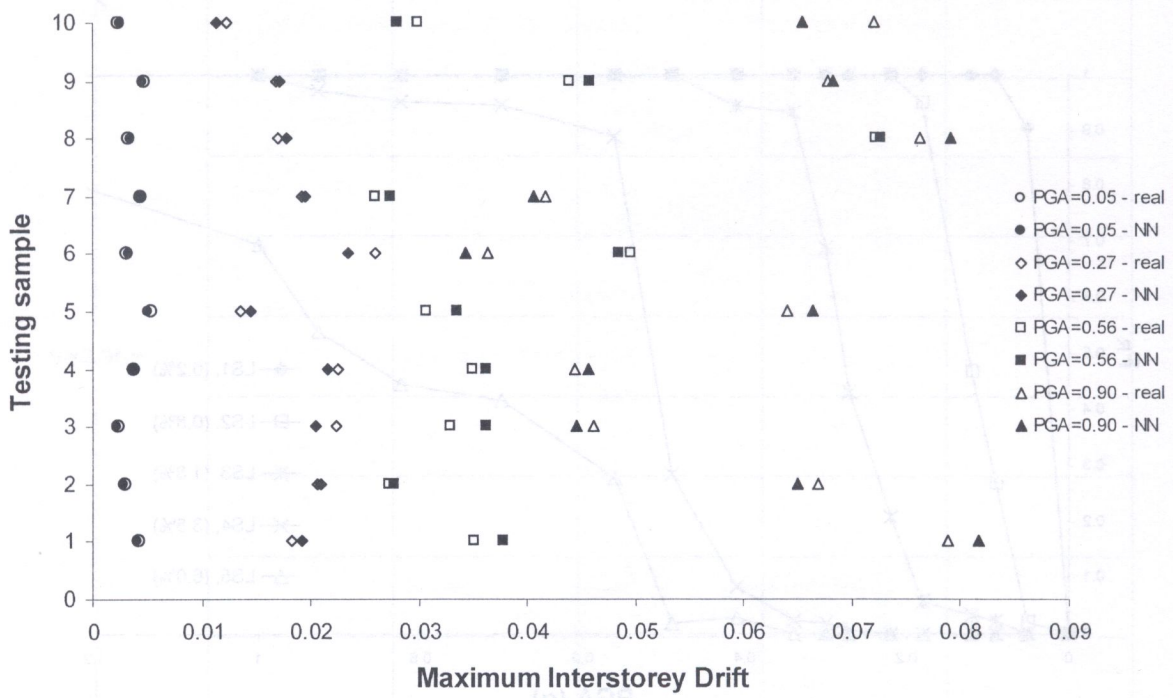

Fig. 8. Prediction of $\theta_{\max}$ for the testing sample

state ($\theta_{\max} \geq 6.0\%$). It can be seen that depending on the calculated probability of exceedance the number of simulations required for a single point of the fragility curve, ranges from 50 to 1000. The validity of the prediction obtained with the NN is shown in Fig. 8. The maximum interstorey drift values predicted for the 10 components of the testing set compared to the values obtained with nonlinear time-history analysis are shown in Fig. 8 for four hazard levels.

8. Metamodel assisted methodology for validating the EC8 approach

Extreme earthquake events may produce extensive damage to structural systems. It is therefore essential to establish a reliable procedure for assessing the seismic risk of real-world structural systems. The reliability of a steel frame designed to EC8 using the modal response analysis as suggested by Eurocode 8 is performed based on the work of Tsompanakis *et al.* [26]. The probability that the life-safety is exceeded is determined, since this is the limit-state that usually controls the design process.

8.1. Structural design under seismic loading based on EC8

The equations of equilibrium for a linearly elastic system in motion can be written in the usual form

$$\mathbf{M}\ddot{\mathbf{u}}(t) + \mathbf{C}\dot{\mathbf{u}}(t) + \mathbf{K}\mathbf{u}(t) = \mathbf{R}(t) \tag{22}$$

where $\mathbf{M}$, $\mathbf{C}$, and $\mathbf{K}$ are the mass, damping and stiffness matrices; $\mathbf{R}(t)$ is the external load vector, while $\mathbf{u}(t)$, $\dot{\mathbf{u}}(t)$ and $\ddot{\mathbf{u}}(t)$ are the displacement, velocity, and acceleration vectors of the finite element assemblage, respectively. The Multi-modal Response Spectrum (MmRS) method is a simplified method for the assessment of seismic demand based on the mode superposition approach. Equation (22) is modified according to the modal superposition approach to a system using the following transformation,

$$\bar{\mathbf{M}}_i\ddot{\mathbf{y}}_i(t) + \bar{\mathbf{C}}_i\dot{\mathbf{y}}_i(t) + \bar{\mathbf{K}}_i\mathbf{y}_i(t) = \bar{\mathbf{R}}_i(t) \tag{23}$$

where

$$\bar{\mathbf{M}}_i = \mathbf{\Phi}_i^T \mathbf{M} \mathbf{\Phi}_i \,, \qquad \bar{\mathbf{C}}_i = \mathbf{\Phi}_i^T \mathbf{C} \mathbf{\Phi}_i \,, \qquad \bar{\mathbf{K}}_i = \mathbf{\Phi}_i^T \mathbf{K} \mathbf{\Phi}_i \qquad \text{and} \quad \bar{\mathbf{R}}_i = \mathbf{\Phi}_i^T \mathbf{R} \tag{24}$$

are the generalized values of the corresponding matrices and the loading vector, while $\mathbf{\Phi}_i$ is the i-th eigenmode shape matrix. According to the modal superposition approach the system of N differential equations, which are coupled with the off-diagonal terms in the mass, damping and stiffness matrices, is transformed to a set of N independent normal-coordinate equations. The dynamic response can therefore be obtained by solving separately for the response of each normal (modal) coordinate and by superposing the response in the original coordinates.

In the MmRS analysis a number of different formulas have been proposed to obtain reasonable estimates of the maximum response based on the spectral values. The simplest and most popular formula for combining the modal responses is the Square Root of Sum of Squares (SRSS). Thus the maximum total displacement is approximated by

$$u_{\max} = \left(\sum_{i=1}^{N} u_{i,\max}^2 \right)^{\frac{1}{2}} \,, \qquad u_{i,\max} = \mathbf{\Phi}_i \, y_{i,\max} \,, \tag{25}$$

where $u_{i,\max}$ corresponds to the maximum displacement vector corresponding to the i-th eigenmode.

8.2. Metamodel assisted methodology

In the present implementation the main objective is to investigate the ability of the NN to predict the structural performance in terms of maximum interstorey drift. The selection of appropriate I/O training data is an important part of the NN training process. Although the number of training patterns may not be the only concern, the distribution of samples is of greater importance. In the present study the sample space for each random variable is divided into equally spaced distances in order to select suitable training pairs. Having chosen the NN architecture and tested the performance of the trained network, predictions of the probability of exceedance of the design limit-state can be made quickly. The results are then processed by means of MCS to calculate the probability of exceedance p_{exceed} of the design limit-state using Eq. (18).

The modulus of elasticity, the dimensions b and h of the I-shape cross-section and the seismic loading have been considered as random variables. Three alternative test cases are considered depending on the random variables considered: (a) the modulus of elasticity and the earthquake loading are considered to be random variables, (b) the dimensions b and h of the I-shape cross section and earthquake loading are taken as random variables and (c) all three groups of random variables are considered together. For the implementation of the NN-based metamodel in all three test cases a two level approximation is employed using two different NN. The first NN predicts the eigenperiod values of the significant modes. The inputs of the NN are the random variables while the outputs are the eigenperiod values. The second NN is used to predict the maximum interstorey drift, which is used to determine whether a limit-state has been violated. Therefore, the spectral acceleration values of both X and Y directions are the input values of the NN while the maximum interstorey drift is the output. The input and output variables for the two levels of approximation are shown in Table 6.

Table 6. Input and output variables for the two levels of approximation

Test case	1st level of approximation (NN1)		1st level of approximation (NN2)	
	Inputs	Outputs	Inputs	Outputs
(a)	E	T_i, $i = 1, \ldots, 8$	$R_{dx}(T_i)$, $R_{dy}(T_i)$, $i = 1, \ldots, 8$	Max drift $\theta_{\max}$
(b)	b_i, h_i, $i = 1, \ldots, 5$	T_i, $i = 1, \ldots, 8$	$R_{dx}(T_i)$, $R_{dy}(T_i)$, $i = 1, \ldots, 8$	Max drift $\theta_{\max}$
(c)	E, b_i, h_i, $i = 1, \ldots, 5$	T_i, $i = 1, \ldots, 8$	$R_{dx}(T_i)$, $R_{dy}(T_i)$, $i = 1, \ldots, 8$	Max drift $\theta_{\max}$

8.3. Seismic probabilistic analysis

The six storey space frame, shown in Fig. 9, has been considered to assess the proposed metamodel-assisted structural probabilistic analysis methodology. The space frame consists of 63 members that are divided into five groups having the following cross sections: (1) IPB 650, (2) IPB 650, (3) IPE 450, (4) IPE 400 and (5) IPB 450. The structure is loaded with a permanent action of $G = 3\,\mathrm{kN/m^2}$ and a live load of $Q = 5\,\mathrm{kN/m^2}$. In order to take into account that structures may deform inelastically under earthquake loading, the seismic actions are reduced using a behavior factor $q = 4.0$ (Eurocode 8, 1994).

The most common way of defining the seismic loading is by means of a regional design code response spectrum. However if higher precision is required the use of spectra derived from natural earthquake records is more appropriate. Therefore, a set of nineteen natural accelerograms, shown in Table 7, is used. The records are scaled, to the same peak ground acceleration of $0.32g$ in order to ensure compatibility. Two are from the 1992 Cape Mendocino earthquake, two are from the 1978 Tabas, Iran earthquake and fifteen are from the 1999 Chi-chi, Taiwan earthquake. The response spectra for each scaled record, in X and Y directions, are shown in Figs. 10 and 11, respectively. In Table 8 the probability density functions, mean values and standard deviations for all random variables are listed.

Each record corresponds to different earthquake magnitudes and soil properties corresponding to different earthquake events. The chosen set is kept in rational size in order to achieve increased efficiency of NN with minimum data and covers, as much as possible, a wide range of excitations in order to provide NN with more "widespread" information as it is well known that NN cannot extrapolate efficiently any given information. Of course, as in any kind of NN application, the selection of approximation data, i.e. the set of records (both the ones for training and the other for NN approximations) in the present application, affects significantly the performance of NN.

Assuming that seismic loading data are distributed lognormally the median spectrum $\hat{x}$ and the standard deviation δ are calculated as follows,

$$\hat{x} = \exp\left[\frac{\sum_{i=1}^{N} \ln(R_{d,i}(T))}{n}\right], \tag{26}$$

$$\delta = \left[\frac{\sum_{i=1}^{N} \left(\ln(R_{d,i}(T)) - \ln(\hat{x})\right)^2}{n-1}\right]^{\frac{1}{2}}, \tag{27}$$

where $R_{d,i}(T)$ is the response spectrum of the i-th record for period value equal to T. The median spectra for both directions are shown in Figs. 10 and 11.

In the first test case one hundred (100) training/testing patterns of the modulus of elasticity are selected in order to train the first NN and one hundred (100) training/testing patterns of the spectral values are selected to train the second NN. Ten out of them are selected to test the efficiency of the trained network. In the second test case the training-testing set was composed by one hundred fifty (150) pairs while in the third test case the set was composed by two hundred (200) pairs while in both cases the second NN is trained using one hundred (100) training/testing patterns. For the six storey frame of Fig. 9, eight modes are required to capture the 90% of the total mass. For each test case a different neural network configuration is used: (i) NN1: 1-10-8, NN2: 16-20-1, (ii) NN1: 10-20-8, NN2: 16-20-1 and (iii) NN1: 11-20-8, NN2: 16-20-1.

The influence of the three groups of random variables with respect to the number of simulations is show in Fig. 12. It can be seen that 2000–5000 simulations are required in order to calculate accurately the probability of exceedance of the design limit-state. The life safety limit-state is considered violated if the maximum interstorey drift exceeds 4.0%.

Once an acceptable trained NN in predicting the maximum drift is obtained, the probability of exceedance for each test case is estimated by means of NN based Monte Carlo Simulation. The

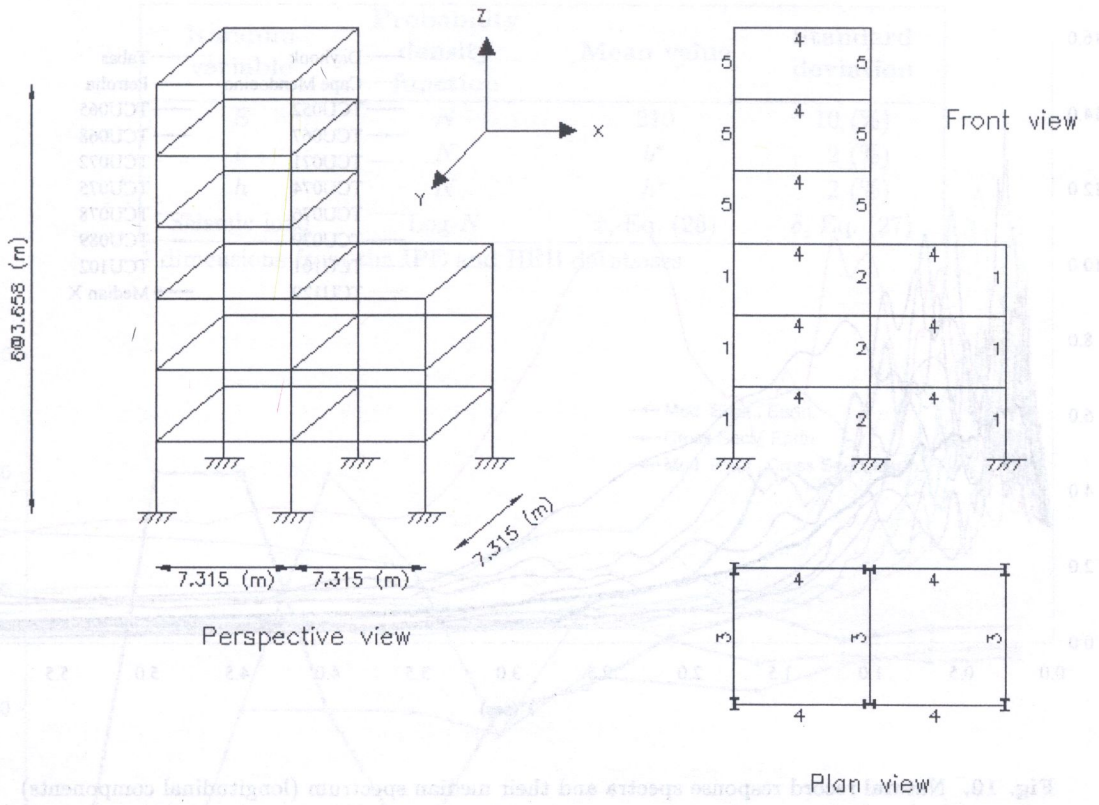

Fig. 9. The six-storey space frame

Table 7. List of the natural records

Earthquake	Station	Distance	Site
Tabas, 16 Sept. 1978	Dayhook	14	rock
	Tabas	1.1	rock
Cape Mendocino, 25 April 1992	Cape Mendocino	6.9	rock
	Petrolia	8.1	soil
Chi-Chi, 20 Sept. 1999	TCU052	1.4	soil
	TCU065	5.0	soil
	TCU067	2.4	soil
	TCU068	0.2	soil
	TCU071	2.9	soil
	TCU072	5.9	soil
	TCU074	12.2	soil
	TCU075	5.6	soil
	TCU076	5.1	soil
	TCU078	6.9	soil
	TCU079	9.3	soil
	TCU089	7.0	rock
	TCU101	4.9	soil
	TCU102	3.8	soil
	TCU129	3.9	soil

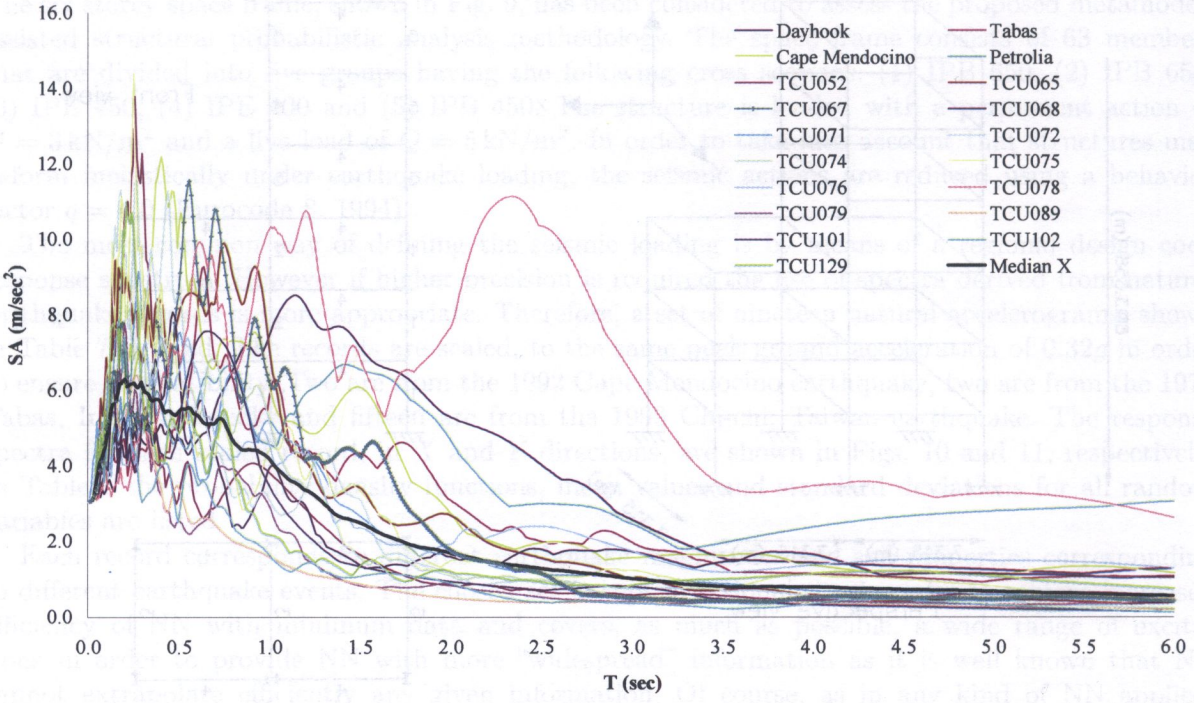

Fig. 10. Natural record response spectra and their median spectrum (longitudinal components)

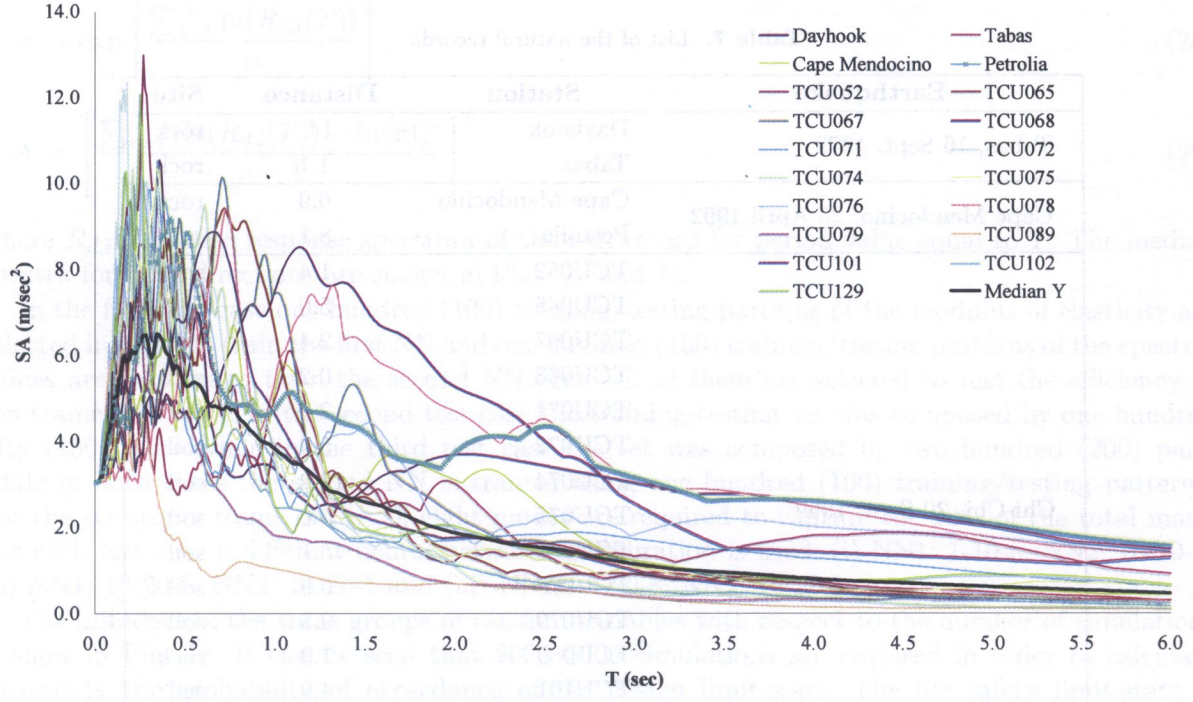

Fig. 11. Natural record response spectra and their median spectrum (transverse components)

Table 8. Characteristics of the random variables

Random variable	Probability density function	Mean value	Standard deviation
E	N	210	10 (%)
b	N	b^*	2 (%)
h	N	h^*	2 (%)
Seismic load	Log-N	$\hat{x}$, Eq. (26)	δ, Eq. (27)

* dimensions from the IPE and HEB databases

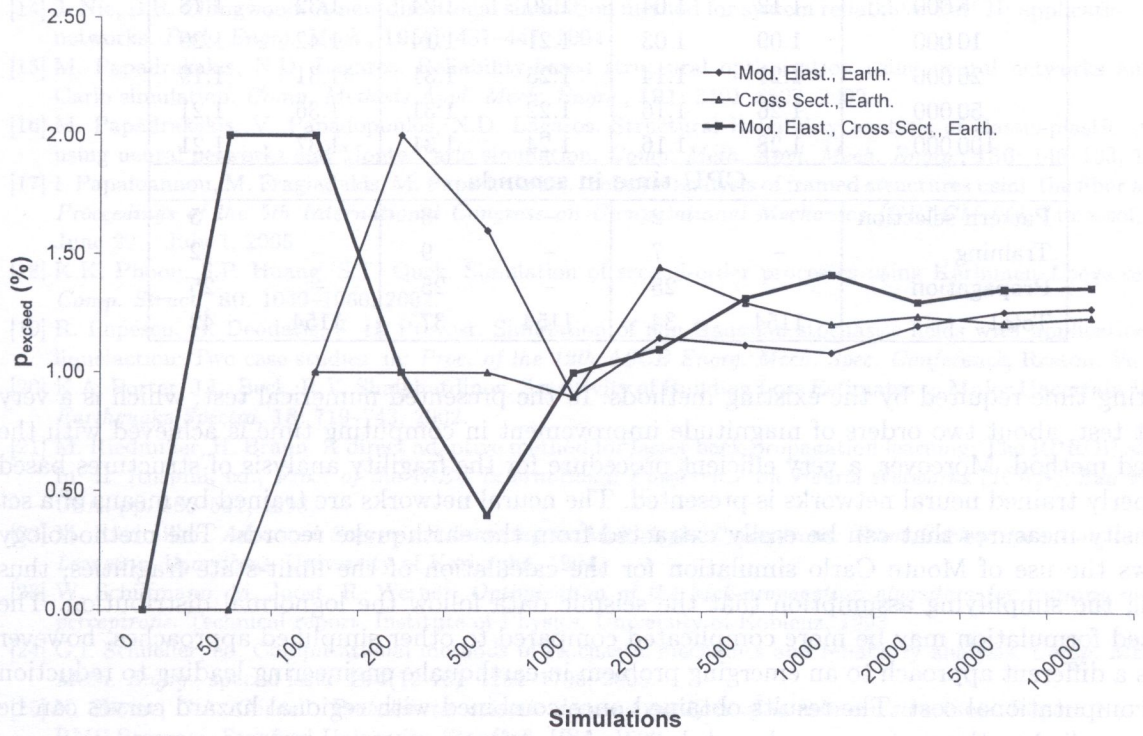

Fig. 12. Influence of the number of MC simulations on the value of p_{exceed} for the three test cases

results for various numbers of simulations are shown in Table 9 for the three test cases examined. It can be seen that the error of the predicted probability of failure with respect to the "exact" one is rather marginal. On the other hand, the computational cost is drastically decreased, approximately 30 times, for all test cases.

9. Conclusions

The implementation of the hybrid simulation method, for the simulation of highly skewed non-Gaussian fields, was found to be very effective. In a stochastic finite element procedure using Monte Carlo simulation, a new non-Gaussian sample function has to be created in every simulation run leading to excessive computational effort in the framework of large-scale structural problems, due to the large sample size and the computing time required for each Monte Carlo run. A computationally efficient non-Gaussian simulation method is therefore crucial for real time stochastic structural analysis. The presented methodology is an efficient, robust and generally applicable procedure capable of simulating highly skewed narrow-banded non-Gaussian fields. Additionally, it was found that the hybrid method can perform the simulation of non-Gaussian fields at a fraction of the

Table 9. "Exact" and predicted values of p_{exceed} and the required CPU time

Number of simulations	Test case 1		Test case 2		Test case 3	
	"exact"	NN	"exact"	NN	"exact"	NN
	p_{exceed}	p_{exceed}	p_{exceed}	p_{exceed}	p_{exceed}	p_{exceed}
50	0.00	0.00	0.00	0.00	2.00	0.00
100	1.00	2.00	1.00	2.00	2.00	1.00
200	2.00	1.60	1.00	1.00	1.00	3.00
500	1.60	1.26	1.00	1.70	0.40	0.70
1 000	0.90	0.81	0.90	0.67	1.00	0.86
2 000	1.15	1.06	1.45	1.41	1.10	0.97
5 000	1.12	1.04	1.30	1.24	1.32	1.18
10 000	1.09	1.03	1.21	1.14	1.42	1.29
20 000	1.21	1.14	1.25	1.31	1.31	1.19
50 000	1.26	1.16	1.22	1.31	1.36	1.21
100 000	1.28	1.16	1.24	1.31	1.37	1.21
CPU time in seconds						
Pattern selection	–	2	–	3	–	5
Training	–	7	–	9	–	12
Propagation	–	25	–	25	–	25
Total	1154	34	1154	37	1154	42

computing time required by the existing methods. In the presented numerical test, which is a very difficult test, about two orders of magnitude improvement in computing time is achieved with the proposed method. Moreover, a very efficient procedure for the fragility analysis of structures based on properly trained neural networks is presented. The neural networks are trained by means of a set of intensity measures that can be easily extracted from the earthquake records. The methodology of allows the use of Monte Carlo simulation for the calculation of the limit-state fragilities, thus avoiding the simplifying assumption that the seismic data follow the lognormal distribution. The presented formulation may be more complicated compared to other simplified approaches, however it offers a different approach to an emerging problem in earthquake engineering leading to reduction of the computational cost. The results obtained once combined with regional hazard curves can be directly applied to the performance-based design of steel frames.

Acknowledgments

This work has been partially supported by the research project "Konstantinos Karatheodori" of the National Technical University of Athens. This support is gratefully acknowledged.

References

[1] G. Deodatis, R.C. Micaletti. Simulation of highly skewed non-Gaussian stochastic processes. *J. Engrg. Mech. (ASCE)* **127**: 1284–1295, 2001.

[2] S. Fahlman. *An Empirical Study of Learning Speed in Back-Propagation Networks.* Carnegie Mellon: CMU-CS-88-162, 1988.

[3] M. Grigoriu. Crossings of non-Gaussian translation processes. *J. Engrg. Mech. (ASCE)*, **110**: 610–620, 1984.

[4] M. Grigoriu. Simulation of stationary non-Gaussian translation processes. *J. Engrg. Mech. (ASCE)*, **124**: 121–126, 1998.

[5] K.R. Gurley, M. Tognarelli, A. Kareem. Analysis and simulation tools for wind engineering. *Prob. Engrg. Mech.*, **12**: 9–31, 1997.

[6] M. Fragiadakis, N.D. Lagaros, M. Papadrakakis, Risk assessment of structures using neural networks. *Proceedings of the 5th International Congress on Computational Mechanics (GRACM 05)*, Limassol, Cyprus, June 29 – July 1, 2005.

[7] J.E. Hurtado, D.A. Alvarez. Neural-network-based reliability analysis: a comparative study. *Comp. Meth. Appl. Mech. Engrg.*, **191**: 113–132, 2002.

[8] J.E. Hurtado, Neural network in stochastic mechanics. *Arch. Comp. Meth. Engrg. (State of the Art Reviews)*, **8**(3): 303–342, 2001.

[9] S.L. Kramer, *Geotechnical Earthquake Engineering.* Prentice-Hall, Englewood Cliffs, NJ, 1996.

[10] N.D. Lagaros, M. Papadrakakis. Learning improvement of neural networks used in structural optimization. *Adv. Engrg. Software*, **35**: 9–25, 2004.

[11] N.D. Lagaros, G. Stefanou, M. Papadrakakis. An enhanced hybrid method for the simulation of highly skewed non-Gaussian stochastic fields. *Comp. Meth. Appl. Mech. Engrg.*, **194**(45-47): 4824–4844, 2005.

[12] F. Masters, K.R. Gurley. Non-Gaussian simulation: Cumulative distribution function map-based spectral correction. *J. Engrg. Mech. (ASCE)*, **129**: 1418–1428, 2003.

[13] D.S. McCorkle, K.M. Bryden, C.G. Carmichael. A new methodology for evolutionary optimization of energy systems. *Comp. Meth. Appl. Mech. Engrg.*, **192**: 5021–5036, 2003.

[14] J. Nie, B.R. Ellingwood. A new directional simulation method for system reliability. Part II: application of neural networks. *Prob. Engrg. Mech.*, **19**(4): 437–447, 2004.

[15] M. Papadrakakis, N.D. Lagaros. Reliability-based structural optimization using neural networks and Monte Carlo simulation. *Comp. Methods Appl. Mech. Engrg.*, **191**: 3491–3507, 2002.

[16] M. Papadrakakis, V. Papadopoulos, N.D. Lagaros. Structural Reliability analysis of elastic-plastic structures using neural networks and Monte Carlo simulation. *Comp. Meth. Appl. Mech. Engrg.*, **136**: 145–163, 1996.

[17] I. Papaioannou, M. Fragiadakis, M. Papadrakakis. Inelastic analysis of framed structures using the fiber approach. *Proceedings of the 5th International Congress on Computational Mechanics (GRACM 05)*, Limassol, Cyprus, June 29 – July 1, 2005.

[18] K.K. Phoon, S.P. Huang, S.T. Quek. Simulation of second-order processes using Karhunen–Loève expansion. *Comp. Struct.*, **80**: 1049–1060, 2002.

[19] R. Popescu, G. Deodatis, J. H. Prevost. Simulation of non-Gaussian stochastic fields with applications to soil liquefaction: Two case studies. in: *Proc. of the 12th ASCE Engrg. Mech. Spec. Conference*, Reston, Va., 1998.

[20] K.A. Porter, J.L. Beck, R.V. Shaikhutdinov. Sensitivity of Building Loss Estimates to Major Uncertain Variables. *Earthquake Spectra*, **18**: 719–743, 2002.

[21] M. Riedmiller, H. Braun. A direct adaptive method for faster back-propagation learning: The RPROP algorithm. In: H. Ruspini, ed., *Proc. of the IEEE International Conference on Neural Networks (ICNN)*, San Francisco, USA, pp. 586–591, 1993.

[22] M. Riedmiller. *Advanced Supervised Learning in Multi-layer Perceptrons: From Back-propagation to Adaptive Learning Algorithms.* University of Karlsruhe, 1994.

[23] W. Schiffmann, M. Joost, R. Werner. *Optimization of the back-propagation algorithm for training multi-layer perceptrons.* Technical report, Institute of Physics, University of Koblenz, 1993.

[24] G.I. Schuëller, ed. Computational methods in stochastic mechanics and reliability analysis. *Comp. Meth. Appl. Mech. Engrg.*, special issue **194**(12-16): 1251–1795, 2005.

[25] N. Shome, C.A. Cornell. *Probabilistic seismic demand analysis of non-linear structures.* Report No. RMS-35, RMS Program, Stanford University, Stanford, USA, 1999.

[26] Y. Tsompanakis, N.D. Lagaros, G.E. Stavroulakis, Efficient neural network models for structural reliability analysis and identification problems. *8th International Conference on the Application of Artificial Intelligence to Civil, Structural and Environmental Engineering (AICC 2005)*, Rome, Italy, August 30 – September 2, 2005.

[27] D. Vamvatsikos, C.A. Cornell. Incremental dynamic analysis. *Earth Engrg. Struct. Dyn.*, **31**: 491–514, 2002.

[28] F. Yamazaki, M. Shinozuka. Digital generation of non-Gaussian stochastic fields. *J. Engrg. Mech. (ASCE)*, **114**: 1183–1197, 1988.

[29] J. Zacharias, C. Hartmann, A. Delgado. Damage detection on crates of beverages by artificial neural networks trained with finite-element data. *Comp. Meth. Appl. Mech. Engrg.*, **193**: 561–574, 2004.

[30] Z. Waszczyszyn, M. Bartczak. Neural prediction of buckling loads of cylindrical shells with geometrical imperfections. *Int. J. Nonlinear Mech.*, **37**(4): 763–776, 2002.

[31] A. Zerva. Seismic ground motion simulations from a class of spatial variability models. *Earth Engrg. Str. Dyn.*, **21**: 351–361, 1992.